Quaternary Science Reviews 144 (2016) 1–15

Contents lists available at ScienceDirect

Quaternary Science Reviews

journal homepage: www.elsevier.com/locate/quascirev

Magnetostratigraphy of a long Quaternary sediment core in the South Yellow Sea

Jianxing Liu [a, b, c, d], Qingsong Liu [c, d, *], Xunhua Zhang [b, **], Jian Liu [b, d], Zhiqiang Wu [b], Xi Mei [b, d], Xuefa Shi [a, d], Quanhong Zhao [e]

[a] Key Laboratory of Marine Sedimentology and Environmental Geology, First Institute of Oceanography, State Oceanic Administration, Qingdao, 266061, People's Republic of China
[b] Qingdao Institute of Marine Geology, Qingdao, 266071, People's Republic of China
[c] State Key Laboratory of Lithospheric Evolution, Institute of Geology and Geophysics, Chinese Academy of Sciences, Beijing, 100029, People's Republic of China
[d] Laboratory for Marine Geology, Qingdao National Laboratory for Marine Science and Technology, Qingdao, 266061, People's Republic of China
[e] State Key Laboratory of Marine Geology, Tongji University, Shanghai, 200092, People's Republic of China

ARTICLE INFO

Article history:
Received 4 January 2016
Received in revised form
9 May 2016
Accepted 18 May 2016
Available online 27 May 2016

Keywords:
Continental shelf
The South Yellow Sea
Core CSDP-1
Greigite
Magnetostratigraphy
Quaternary
Sedimentary evolution

ABSTRACT

Continental shelves serve as a bridge between the continent and ocean and sediments in this region are sensitive to land-sea interaction, sea-level variation and local subsidence. In this study, we present a comprehensive magnetic study of the longest sediment core (CSDP-1, 300.1 m) recovered from the South Yellow Sea. The major magnetic minerals in the studied sediments are magnetite, hematite and greigite. Greigite records a chemical remanent magnetization, which can be removed effectively by thermal demagnetization. The magnetostratigraphy defined in this study contains the Matuyama-Brunhes boundary (M/B, 781 ka) at ~73.68 m, which is consistent with results from adjacent cores. The base of the Quaternary (~2.6 Ma) in the Yellow Sea is recovered for the first time at a depth of 227.16 m. The basal age of the core is estimated to be ~3.50 Ma. It indicates that the first transgression of the Yellow Sea occurred no later than ~1.7 Ma. Succeeding large amplitude regressions occurred in some cold periods such as during MIS 20, MIS 18, and MIS 10. Our results provide the first chronology that brackets the entire Quaternary and we reconstruct the sedimentary evolution of the Yellow Sea with robust age constraints, which provides an important framework for further paleoenvironmental and tectonic studies.

1. Introduction

Continental shelves are among the most active regions for land-sea interaction in the Earth System (McMillan, 2002), and are typically important for economic production and for human recreational activities (Eckert, 1979). Sediments from the continental shelf are highly sensitive to sea-level fluctuations, climate changes, and local subsidence (Troiani et al., 2011). Fluvial material that is transported to this region can either accumulate or be re-transported to the ocean depending on the accommodation space that is controlled by both sea-level and tectonic subsidence (Gerber et al., 2010; Yao et al., 2014). Sedimentation rates on the continental shelf are usually much higher than those in the deep sea, which makes shelf sediments suitable for high-resolution studies (e.g., Liu et al., 2004).

The Yellow Sea (Fig. 1) is a typical continental shelf with extensive area in the east of China. Deposited under relatively shallow water depths (44 m on average), sediment sequences in this region are highly sensitive to sea-level fluctuations as a result of Quaternary glacial-interglacial cycles as well as local tectonics (Qin et al., 1989; Yang et al., 1996). In addition, it is an important sediment reservoir for two globally large rivers, the Yellow River and Yangtze (Changjiang) River, and other small rivers on the Korean Peninsula (Yang et al., 2003). Therefore, sediments from the

* Corresponding author. State Key Laboratory of Lithospheric Evolution, Institute of Geology and Geophysics, Chinese Academy of Sciences, Beijing, 100029, People's Republic of China.
** Corresponding author. Qingdao Institute of Marine Geology, Qingdao, 266071, People's Republic of China
E-mail addresses: qsliu@mail.iggcas.ac.cn (Q. Liu), xunhuazh@vip.sina.com (X. Zhang).

http://dx.doi.org/10.1016/j.quascirev.2016.05.025
0277-3791/

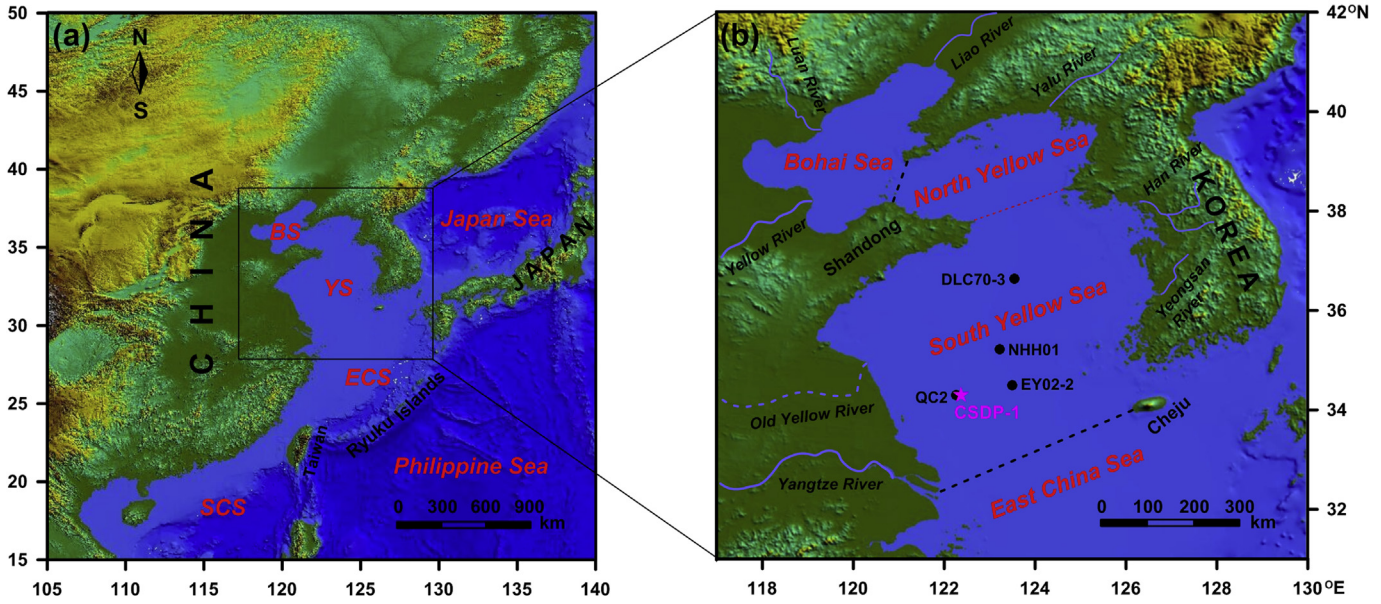

Fig. 1. (a). Schematic map of the marginal sea distribution in the northwest Pacific Ocean (BS: the Bohai Sea; YS: the Yellow Sea; ECS: the East China Sea; SCS: the South China Sea). (b). Map of the Yellow Sea and adjacent areas, with locations of existing long sediment cores, and the cores QC2, EY02-2, NHH01, DLC70-3 are from Zhou and Ge (1990), Ge et al. (2006), Liu et al. (2014a), and Mei et al. (2016), respectively.

Yellow Sea will contain important paleoenvironmental information that is relevant to studying sea-level and tectonic variations, source to sink processes, and East Asian monsoon evolution (Liu et al., 2014a). Nevertheless, most previous studies have focused on shorter time-scales over the last interglacial, such as evolution of the Yellow River subaqueous delta during the Holocene (Yang and Liu, 2007), marine isotope stage (MIS) 3 to MIS 2 (Liu et al., 2010), and the paleoenvironmental history of the central South Yellow Sea (SYS) mud area since the early Holocene (Xiang et al., 2008). Studies on longer time-scales are relatively scarce due to the lack of reliable chronological frameworks.

For long-core sediment sequences, magnetostratigraphy is one of the most efficient ways to establish a reliable first-order chronological framework (e.g., Lanci et al., 2004; Tauxe et al., 2012). So far, magnetostratigraphic studies have been reported for four long cores (QC2, EY02-2, NHH01, and DLC70-3) (Fig. 1b; Table 1) from the Yellow Sea. The 108.83-m QC2 core contains the Matuyama-Brunhes boundary (M/B: ~781 ka B.P.) at 79.95 m (or ~63 m after removing the ~17-m-thick Holocene sand ridge) and a basal age of ~1.8 Ma (Zhou and Ge, 1990). The M/B boundary of core EY02-2, which has a total length of 70 m, was identified at 63.29 m, and its basal age was extrapolated to ~0.9 Ma (Ge et al., 2006). Recent studies have located the M/B boundary in the 125.64-m NHH01 core at 68.64 m with a linearly extrapolated basal age of ~1.06 Ma (Liu et al., 2014a), and the M/B boundary of the 71.2-m DLC70-3 core at 59.08 m (Mei et al., 2016).

Quaternary climate is characterized by glacial and interglacial alternations that have resulted in large-scale sea-level oscillations that influenced the architecture of continental shelf sediments (Yao et al., 2014). Numerous sediment cores from the Yellow Sea and its surrounding coastal plains have revealed that sedimentation in this region is characterized by alternation of marine and lacustrine/terrestrial deposits (Qin et al., 1989). In core QC2 (Fig. 1b), seven marine transgressions divide the recorded paleogeographic evolution into four periods since the Olduvai subchron (Yang, 1993). Comprehensive analyses of seismic profiles and sediment cores from the western SYS reveal that sedimentary environmental changes since MIS 5 were strongly controlled by sea-level fluctuations, with most of the preserved sediments deposited in MIS 5, MIS 3, and MIS 1 and major erosion events in MIS 4 and MIS 2 (Liu et al., 2010). Using foraminifera abundances, eight transgression layers have been identified in core DLC70-3 (Fig. 1b) (Mei et al., 2016). In short, great progress has been made in understanding the sedimentary evolution of the Yellow Sea since the middle Pleistocene, especially over the late Pleistocene. However, the sedimentary evolution history throughout the Quaternary is still not well understood.

In this study, we investigated a 300.1-m-long sediment core from the SYS. Detailed rock magnetic and high-resolution paleomagnetic investigations are presented along with a robust chronology that brackets the entire Quaternary for the SYS. We use this paleoenvironmental reconstruction to outline the sedimentary history of the SYS.

2. General setting

The Bohai Sea, Yellow Sea, and the East China Sea together constitute a marginal sea bounded by China, Korea, and southern

Table 1
Detailed information on long sediment cores from the South Yellow Sea.

Core ID	Water depth/m	Drilling depth/m	Recovery rate/%	Location longitude/latitude	Drilling time
QC2	49.05	108.83	90.4	122°16′E/34°18′N	May, 1984
EY02-2	79.00	70.00	86.5	123°30′E/34°30′N	February, 2001
NHH01	73.00	125.64	91.0	123°13′E/35°13′N	June, 2009
DLC70-3	73.00	71.20	93.0	123°33′E/36°38′N	September, 2009
CSDP-1	52.50	300.10	80.0	122°22′E/34°18′N	June, 2013

Japan, and is separated from the western North Pacific Ocean by the Ryukyu Island arc and Taiwan (Fig. 1a, Liu et al., 2010). More than 70% of this marginal sea is occupied by a broad continental shelf that is the seventh largest in the world with water depths of less than ~150 m. The Yellow Sea is a typical semi-enclosed (open to the southeast) epicontinental sea that rests on a flat and tectonically stable seafloor, with average and maximum water depths of ~44 m and 140 m, respectively (Yang et al., 2003; Liu et al., 2014a). It is located between the Chinese mainland and Korean Peninsula, it stretches 870 km from north to south and 556 km from east to west, and it has an area of ~380,000 km^2 (He, 2006).

The link between the Chengshan Cape of Shandong Peninsula and Changsangot of the Korean Peninsula divides the Yellow Sea into the North Yellow Sea (NYS) and SYS. The NYS is separated from the Bohai Sea at its western extremity by Liaotieshan Cape of Liaodong Peninsula and Penglai Cape of Shandong Peninsula, while the SYS is bounded in the south with the East China Sea by an arbitrary line that connects the Yangtze River Estuary and Cheju Island (Fig. 1b, Qin et al., 1989). Water depths in the NYS are generally less than 60 m with an average of 38 m, and the SYS is mostly less than 100 m deep with an average water depth of 46 m. The SYS has a maximum width of ~700 km and deepens toward the Yellow Sea Trough, which is defined by the 80-m isobath and extends NW-SE (Liu et al., 2010).

The SYS basin has undergone extensive subsidence during the Cenozoic so that it contains an enormous thickness of sediments, with Quaternary sediments having thickness of up to 300 m (Qin et al., 1989). Mineralogical and geochemical studies of the surface sediments indicate that the major source of sediments to the western and middle part of the Yellow Sea are the Yellow River and Yangtze River, while Korean rivers dominate in the east (Lan et al., 2005).

3. Material and methods

3.1. Core description

The studied core CSDP-1 (122°22′ E, 34°18′ N, Fig. 1b; Table 1) was recovered from the western SYS at a water depth of ~52.5 m. Core CSDP-1 is the first borehole of the "China Continental Shelf Drilling Program" that started in 2011 and is also the longest sediment core recovered from the SYS so far. The core was recovered using rotary drilling method in June, 2013, with a total drilling length of 300.1 m and an average recovery rate of 80%.

The recovered core was split equally into two halves, which were subsequently photographed and described. The archive half was preserved in a 4 °C repository and the working half was sampled. According to core observations and descriptions, silt and clayey silt dominate the sediment sequence, with occasional interbedded medium-coarse sand/gravel layers. Marine sediments are only identified in the upper half of the core, mainly in the upper 85 m of the recovered section.

3.2. Rock magnetic experiments

Hysteresis loops were measured on 567 samples at ~0.5 m intervals using a Princeton Measurements Corporation vibrating sample magnetometer (VSM, MicroMag 3900). The magnetic field was cycled between +1.5 T and −1.5 T, with a field increment of 5 mT and an averaging time of 300–500 ms. Saturation magnetization (M_s), saturation remanence (M_{rs}), and coercivity (B_c) were determined after paramagnetic slope correction. Specimens were then demagnetized in alternating fields up to 1.5 T, and an isothermal remanent magnetization (IRM) was imparted stepwise from 0 to 1.5 T. Finally, backfields were applied stepwise up to −1.0 T to the magnetically saturated specimens to obtain the coercivity of remanence (B_{cr}). For representative samples, first-order reversal curves (FORCs) were also measured using the VSM 3900, with 100 FORCs measured at fields up to 1.5 T and an averaging time of 500 ms. FORC diagrams (Pike et al., 1999) were then processed using the FORCinel software of Harrison and Feinberg (2008).

Temperature-dependent curves of magnetic susceptibility (χ-T, mass specific) were measured for 16 representative samples using a Kappabridge MFK1-FA system with a CS-3 high-temperature furnace (Agico Ltd., Brno) from room temperature to 700 °C in an argon atmosphere (Hrouda, 1994). At parallel depths, cubic samples were subjected to analysis of thermal demagnetization of three-component IRMs following Lowrie (1990). The samples were magnetized in successively smaller fields along three mutually orthogonal axes using a 2-G Enterprises Pulse Magnetizer (2G660), with a 2.5 T induction along the z-axis (high-coercivity fraction), 0.5 T along the y-axis (medium-coercivity fraction), and 0.05 T along the x-axis (low-coercivity fraction), respectively. Then samples were subjected to progressive thermal demagnetization up to 690 °C at 20–50 °C intervals.

Low-temperature measurements were conducted on splits of these representative samples using a Quantum Design Magnetic Property Measurement System (MPMS-5XL). Samples were first cooled from 300 K to 20 K in zero field, then an IRM was imparted in a field of 2.5 T. After removal of the field, the IRM was thermally demagnetized by sweeping the temperature from 20 K to 300 K at 5 K/min.

Anistropy of magnetic susceptibility (AMS) for all paleomagnetic samples was measured using a KLY-4s Kappabridge instrument before the samples were subjected to demagnetization. AMS can be described in terms of an ellipsoid with three mutually orthogonal susceptibility axes that are designated the maximum (K_1), intermediate (K_2), and minimum (K_3) axes. These quantities can be combined variously to describe the shape of the ellipsoid and the features of the corresponding magnetic fabric (Hrouda, 1982). The major AMS parameters examined in this study are the lineation (L, defined as $L = K_1/K_2$) and foliation (F, defined as $F = K_2/K_3$).

3.3. Paleomagnetic measurements

Stepwise alternating field (AF) demagnetization of the natural remanent magnetization (NRM) was performed on 2153 cubic samples at a sampling interval of ~0.1 m using a 2-G Enterprises Model 760-R cryogenic magnetometer (2G760) installed in a magnetically shielded (<300 nT) space. AF demagnetization steps of 5–10 mT were used up to a maximum AF of 100 mT.

Thermal demagnetization of the NRM and remanence measurements were carried out on 523 samples collected with 2 × 2 × 2 cm nonmagnetic quartzose boxes at ~0.5 m sampling intervals also in the magnetically shielded laboratory. The samples were heated to a maximum temperature of 690 °C at 20–50 °C intervals in a self-made thermal demagnetizer (PGL100) with much higher thermal stability and lower residual field (AC current field is ~800 nT) than similar commercially available instruments (e.g., AC current field of TD48 is ~80 μT) (Zheng et al., 2010). Remanence was measured in a 2-G Enterprises Rapid System in which the minimum background measurements (~1 × 10^{-12} Am^2) are much smaller than for conventional magnetometers. All magnetic measurements were accomplished in the Paleomagnetism and Geochronology Laboratory, Institute of Geology and Geophysics, Chinese Academy of Sciences.

4. Results

4.1. Rock magnetism

Hysteresis loops, IRM acquisition curves and FORC diagrams were used to assess the magnetic mineralogy of the studied sediments (Fig. 2). For the majority of samples, their hysteresis loops are closed prior to 0.5 T (e.g., Fig. 2a–c) and the corresponding IRM acquisition curves are almost saturated at ~0.3 T (e.g., Fig. 2e–g), which indicates that low-coercivity minerals dominate the magnetic mineral assemblages. Some samples have relatively higher B_c values (25–56 mT) with B_{cr}/B_c ~1.5 and M_{rs}/M_s ~0.5 (e.g., Fig. 2a, b), which is indicative of typical single-domain (SD) behavior. In addition, the corresponding FORC diagrams of these samples are characterized by closed concentric contours about a central peak, a negative region in the lower left-hand part of the diagram, a peak value of 60–70 mT for B_c, and an evident spread in the B_u direction (e.g., Fig. 2i, j). All of these lines of evidence indicate the presence of authigenic SD greigite (e.g., Roberts, 1995; Sagnotti et al., 2010; Roberts et al., 2006, 2011; Liu et al., 2014b). In contrast, FORC diagrams for other samples are typical of low-coercivity SD-PSD (pseudo-single domain) and/or PSD-MD (multi-domain) magnetic minerals (Roberts et al., 2000, 2014; Muxworthy and Dunlop, 2002; Qin et al., 2008) (e.g., Fig. 2k). For some samples with low magnetization, hysteresis loops are wasp-waisted and are still not saturated at high fields (e.g., Fig. 2d). Together with unsaturated IRM acquisition curves (e.g., Fig. 2h) up to 1.5 T, this suggests the coexistence of high- (e.g., hematite) and low-coercivity (e.g., magnetite) phases (Roberts et al., 1995). FORC diagrams for this kind of sample are noisy and only contain a weak signal associated with the low-coercivity component (e.g., Fig. 2l).

Temperature-dependent magnetic susceptibility (χ-T) measurements can be further used to determine magnetic minerals in samples (Hrouda, 1994; Dunlop and Özdemir, 1997). χ-T curves for most samples are characterized by a marked drop in χ at about 585 °C (e.g., Fig. 3a–c), the Curie point of magnetite. Other χ-T curves contain a major drop at about 680 °C (e.g., Fig. 3d), which is characteristic of hematite. In addition, increased χ on heating from about 350 °C in some samples (e.g., Fig. 3a–c) likely results from neoformation of strong ferrimagnetic minerals via alteration of iron-containing silicates/clays (e.g., Hirt and Gehring, 1991; Hirt et al., 1993) and/or paramagnetic iron sulfides such as pyrite (e.g., Passier et al., 2001) which usually coexists with greigite (e.g., Roberts et al., 2011). The cooling cycles of χ-T curves for all samples

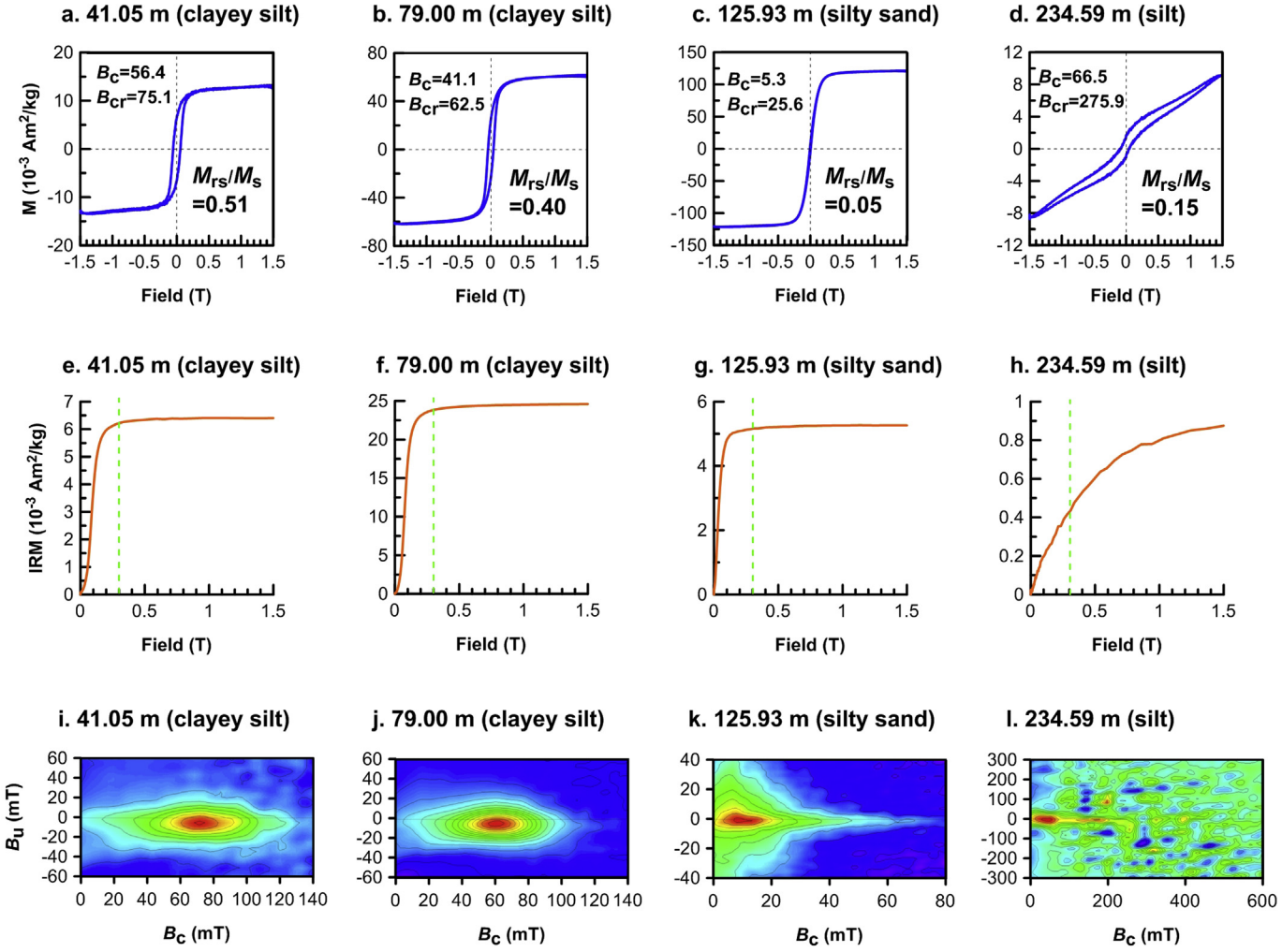

Fig. 2. Rock magnetic results for representative samples, including (a–d) hysteresis loops after paramagnetic slope correction, (e–h) IRM acquisition curves, and (i–l) first-order reversal curve (FORC) diagrams which are obtained by measuring 100 FORCs in an applied field up to 1.5 T and an averaging time of 500 ms, and then calculated with a smoothing factor (SF) of 5. The hysteresis loops and IRM curves are obtained in an applied field up to 1.5 T, with a field increment of 5 mT and an averaging time of 300 ms, and the unit for B_c and B_{cr} in (a–d) is mT.

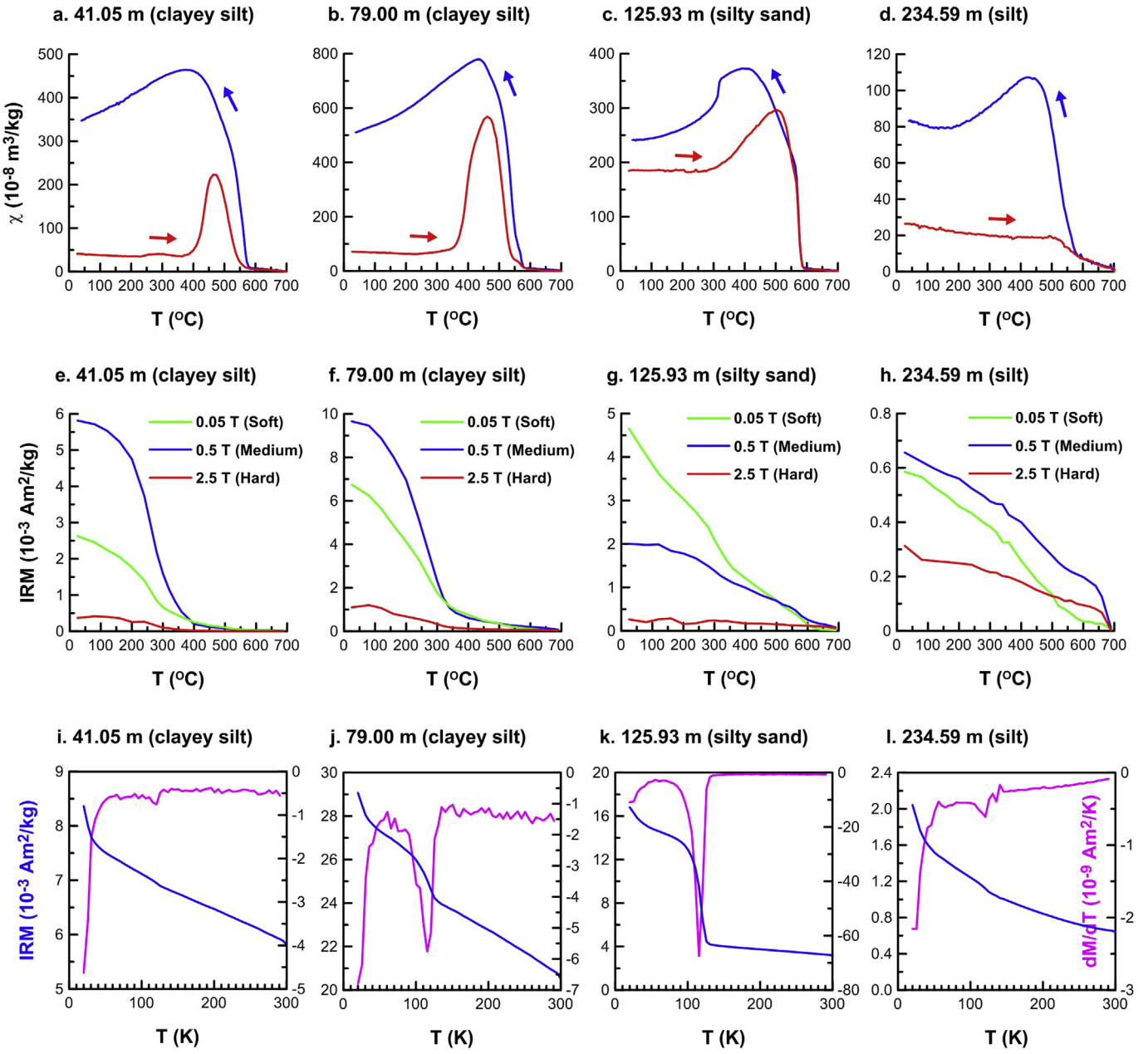

Fig. 3. Rock magnetic results for representative samples, including (a–d) temperature-dependent curves of magnetic susceptibility (χ-T), (e–h) thermal demagnetization of three-component IRMs (Lowrie, 1990) produced by magnetizing specimens in 2.5, 0.5 and 0.05 T along the z-, y-, and x-axes, respectively, and (i–l) low-temperature curves for an IRM (mass specific) acquired at 20 K by applying a 2.5-T field and then observed at 5 K intervals to 300 K during zero-field warming (blue lines), with first-order derivative of magnetizations with respect to temperature (dM/dT) ploted on the right y-axes (magenta lines). The red and blue lines in (a–d) denote heating and cooling curves, respectively. (For interpretation of the references to color in this figure caption, the reader is referred to the web version of this article.)

increase when cooled below 585 °C (Fig. 3a–d), which indicates that magnetite was produced during the heating/cooling process.

Thermal demagnetization curves for three-component IRMs indicate that low-, medium- and high-coercivity minerals all contribute to the remanence (Fig. 3e–h). For some samples, the maximum unblocking temperature of the dominant IRM carrier is in the range of 300–400 °C (e.g., Fig. 4e–f), which along with hysteresis parameters (Fig. 3a–b) and FORC diagrams (Fig. 3i, j) undoubtedly indicate the presence of greigite (Chang et al., 2008; Sagnotti et al., 2010; Roberts et al., 2011). The IRM can be fully demagnetized at around 600 °C, which indicates the coexistence of greigite and magnetite. For the other samples, the dominant IRM of some samples is carried by the low- and medium-coercivity components that evidently unblock at ~600 °C (e.g., Fig. 3g), which indicates that magnetite is the dominant magnetic mineral. For the hard-component, the IRM is gradually demagnetized up to ~680 °C (e.g., Fig. 3h), which indicates that contributions from hematite are significant.

Low-temperature measurements on some representative samples contain an evident Verwey transition at 120 K (Verwey, 1939), which indicates the presence of stoichiometric magnetite (e.g., Fig. 3j, k). In contrast, the Verwey transition is highly smeared (e.g., Fig. 3i, l) in other samples, which indicates the minor presence of magnetite. These results are well consistent with those of the

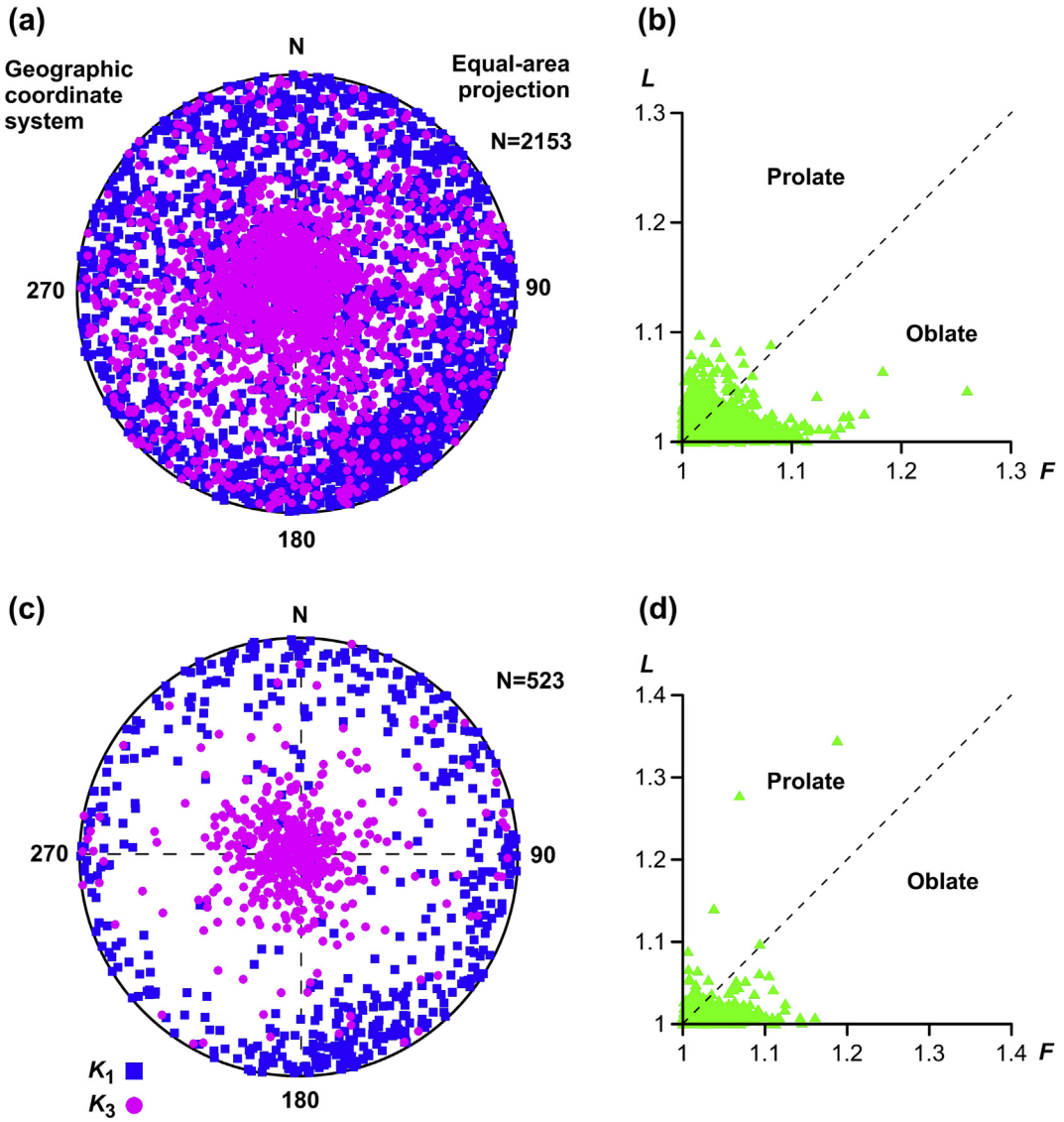

Fig. 4. Anisotropy of magnetic susceptibility (AMS) data for samples subjected to (a,b) AF and (c,d) thermal demagnetization, respectively. (a,c) Projection of axes of maximum (K_1) and minimum (K_3) susceptibility. (b,d) Magnetic lineation (L) versus magnetic foliation (F).

thermal demagnetization of three-component IRMs (Fig. 3e–h).

In the AMS results, L is usually smaller than F, which indicates that the AMS ellipsoid is oblate (Fig. 4b, d). More than 60% of the samples treated with AF demagnetization (Fig. 4a) and 80% of the samples treated with thermal demagnetization (Fig. 4c) have sub-vertical minimum susceptibility axes (K_3) that are almost perpendicular to the bedding plane, while the inclinations of the maximum axes (K_1) are relatively shallow (<20°). These results denote an original sedimentary magnetic fabric that has remained unperturbed since deposition for most samples.

4.2. Paleomagnetism

The characteristic remanent magnetization (ChRM) of the magnetite-dominant samples can be identified mostly between 20 mT and 60 mT for AF demagnetization (e.g., Fig. 5a, d) or between 450 °C and 600 °C for thermal demagnetization (e.g., Fig. 5f, h), respectively. For some greigite-bearing samples, the ChRM could also be isolated using AF demagnetization; at least 80% of NRM was removed below 80 mT (e.g., Fig. 5b-c), whereas the others acquired a spurious gyromagnetic remanent magnetization (GRM) when demagnetized to high fields (Fig. 6a, c) as has been reported widely to be more typical of greigite (e.g., Snowball, 1997; Roberts et al., 2011).

Demagnetization results were evaluated using orthogonal diagrams (Zijderveld, 1967), and each ChRM direction was computed by a "least-squares fitting" technique (Kirschvink, 1980) with at least four successive data points that define a linear trend that is directed clearly to the origin of the orthogonal plot. Samples with maximum angular deviation (MAD) > 15° or/and K_3 inclinations < 50° were excluded. The core was not oriented, so only magnetic inclination (Inc) data were subsequently used to construct a magnetostratigraphy.

Paleomagnetic inclinations calculated from the AFD or thermal demagnetization data prior to 400 °C are usually different from those computed from the thermal demagnetization data above 400 °C in the greigite-dominated samples as we also encountered in core NHH01 (Fig. 1b, Liu et al., 2014a). For example, the paleomagnetic inclinations for some samples have the same direction but distinctly different values (e.g., Fig. 5e) while in other samples,

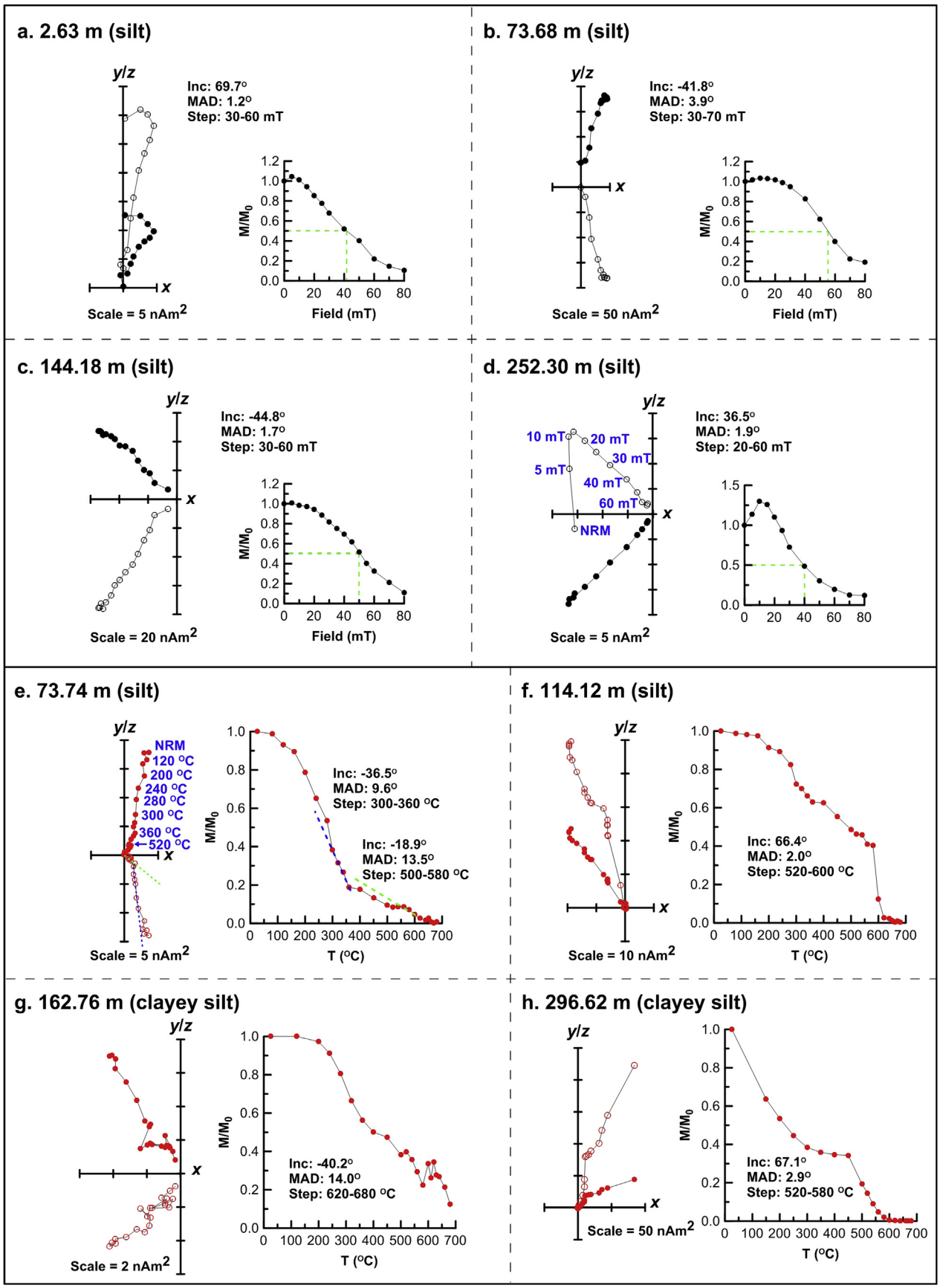

Fig. 5. Orthogonal vector plots (left) and remanence decay curves (right) for (a–d) stepwise AF and (e–h) thermal demagnetization data for representative samples. Solid (open) circles represent projections onto the horizontal (vertical) plane. The green dashed lines in the remanence decay curves in (a–d) denote the median destructive field (MDF). The dashed lines in (e) represent fits to two separate components. The core was not oriented, so no declinations are reported. "Step" indicates the demagnetization range over which the linear component fitting was conducted for each sample. (For interpretation of the references to color in this figure caption, the reader is referred to the web version of this article.)

the inclinations changed sign when heated to ~360 °C (e.g., Fig. 6b, d). Although the Curie temperature of greigite remains unknown but must exceed 350 °C, it will be almost completely demagnetized prior to 400 °C (Roberts et al., 2011). Therefore, the NRM that remains above this temperature interval will be carried only by iron oxides (mainly magnetite).

Three magnetozones are recognized in the core (Fig. 7b): two with normal polarity, N1 (0–73.68 m) identified from thermal demagnetization data above 400 °C or (0–82.80 m) by both AF data and thermal demagnetization data below 400 °C, N2 (227.16–300.10 m); and one with reverse polarity, R1 (73.68–227.16 m) or (82.80–227.16 m) as determined from both demagnetization types. Moreover, eight negative inclination anomalies are recognized within N1 and N2, labeled as r1 (13.47–13.99 m), r2 (18.86–19.25 m), r3 (21.76–23.05 m), r4 (25.75–26.08 m), r5 (41.16–43.28 m), which is not observed in thermal demagnetization data above 400 °C, r6 (57.17–57.96 m), r7 (255.01–257.78 m), and r8 (269.45–272.38 m). R1 is also punctuated by four relatively thin intervals with positive inclinations, which are labeled as n1 (93.08–93.50 m), n2 (111.90–114.26 m), n3 (140.12–140.86 m), and n4 (154.93–160.53 m) in Fig. 7b.

5. Discussion

5.1. Remanence recording mechanism in greigite

Paleoenvironments (e.g., redox conditions) on the Chinese continental shelf change at different time scales due to the combined effects of organic input, sea-level changes and local tectonics (Liu et al., 2014a; Mei et al., 2016). Early diagenetic reactions are the most familiar means by which postdepositional alteration of detrital magnetic minerals (magnetite and hematite) occurs in marine sediments (e.g., Larrasoaña et al., 2007; Fu et al., 2008). It has been reported that non-steady state diagenesis is a major factor in sediments from the continental shelf where large-amplitude sea-level variations give rise to variable changes in organic carbon content, sulphate content and pore water content with time (Roberts, 2015). If such sediments have been subjected to continuous sulphate reduction, detrital magnetic minerals such as magnetite and hematite will dissolve (e.g., Canfield and Berner, 1987). Oscillation between oxic and sulphidic diagenetic conditions is likely in such environments. Accordingly, magnetic mineral assemblages in the sediments of this region are complex and include both primary iron oxides such as magnetite and hematite, and secondary iron sulfides such as greigite (e.g., Oda and Torii, 2004; Nilsson et al., 2013; Liu et al., 2014b).

Authigenic greigite forms in sulfate-reducing sedimentary environments as an intermediate phase during pyritization reactions (e.g., Berner, 1984; Benning et al., 2000). Some studies suggest that pyritization reactions occur during early diagenesis at shallow burial depths and that the persistence of greigite in geological records can provide an approximately syn-depositional paleomagnetic record (e.g., Roberts and Turner, 1993; Reynolds et al., 1999). In contrast, other studies have demonstrated that delayed formation of greigite gives rise to late sedimentary remagnetizations (Florindo and Sagnotti, 1995; Jiang et al., 2001; Roberts and Weaver, 2005). Greigite can authigenically form at various depths below the sediment-water interface during diagenesis, which makes it difficult to ascertain the time at which the chemical remanent magnetization (CRM) was acquired (e.g., Florindo and Sagnotti, 1995; Liu et al., 2004; Roberts et al., 2005; Roberts and Weaver, 2005; Sagnotti et al., 2005, 2010; Roberts, 2015). The timing of greigite formation can vary enough to give contradictory polarities for different generations of greigite even within a single stratigraphic horizon (Jiang et al., 2001). A second possible explanation proposed for the inconsistent remanences is self-reversal of greigite (Horng et al., 1998). However, the physical mechanism for this hypothetical process has remained poorly understood (Florindo and Sagnotti, 1995).

Unlike self-reversal which usually occurs in titanomagnetites and results from exchange interactions within a particle (e.g., O'Reilly and Banerjee, 1966; Schult, 1968), Liu et al. (2014a) proposed that vortex magnetic states in magnetite particles can be expected to realign the magnetization of nearby SD greigite particles and that it could give rise to recording of an opposite polarity direction with respect to the ambient field. Subsequently, the larger magnetite particles might be partially or completely dissolved depending on the supply of sulphide (H_2S or HS^-) that produced by sulphate reduction (Canfield and Berner, 1987; Roberts, 2015), leaving greigite as the major remanence carrier. This model gives rise to "magnetic interaction-induced contradictory magnetization" and predicts that authigenic greigite of either early or late diagenetic origin can record various polarities according to the spatial arrangement of interactions among SD greigite and larger magnetite particles (Liu et al., 2014a).

Greigite in the studied core is authigenic according to the rock magnetic results (see Fig. 2i, j). Greigite-bearing layers (grey bars) (Fig. 7e) often record remanence directions with both the same and opposite polaries with respect to coexisting magnetite or/and hematite (see Figs. 5e–7c), which supports the "magnetic interaction-induced contradictory magnetization" mechanism. Nevertheless, thermal demagnetization can efficiently remove the effects of greigite on paleomagnetic directions, so that only magnetite and hematite signals represent the primary depositional remanent magnetization.

5.2. Magnetostratigraphy and paleoenvironments of the studied core

According to the above analyses, the M/B boundary in the studied core is confidently identified at 73.68 m by combining both AF and thermal demagnetization results, and the major polarity boundary that divides magnetozones R1 and N2 at 227.16 m is correlated to the Gauss-Matuyama boundary (G/M: 2588 ka, the base of the Quaternary) in the GPTS (Gradstein et al., 2012) (Fig. 7a, b). The two relatively thick magnetozones with positive inclinations within R1 (n2 and n4) can be correlated to the Jaramillo (990–1070 ka) and Olduvai (1770–1950 ka) subchrons, respectively (Fig. 7a, b). Since there are only two subchrons with reversed polarity in the Gauss chron (Gradstein et al., 2012), magnetozones r7 and r8 are correlated to the Kanea (3040–3110 ka) and Mammoth (3220–3330 ka) subchrons, respectively. On the basis of this correlation, an age of ~3.5 Ma was linearly extrapolated for the base of the core (Fig. 7a, b). In the Quaternary, the sediments have a mean sedimentation rate of 8.78 cm/kyr (Fig. 8), which is comparable to estimated values on 1000-year time scales during the late Quaternary (Kim et al., 1999). In addition, assuming uniform sedimentation rates during each period (Fig. 8), some of short-lived inclination anomalies in the studied core are also tentatively correlated to the excursions that are well validated (Laj and Channell, 2007; Roberts, 2008) (Fig. 7a, b).

The reliability of the magnetostratigraphy for core CSDP-1 can be further assessed by comparison with nearby cores. Regardless of the variable thickness of Holocene deposits, which range from ~17-m in QC2 (Zhou and Ge, 1990), ~2-m in EY02-2 (Ge et al., 2006), ~4.5-m in NHH01 (Liu et al., 2014a), 0-m in DLC70-3 (Mei et al., 2016), and ~3-m in CSDP-1, the thickness of sediments deposited since the mid-Pleistocene (0.78 Ma) in these cores are consistently 60–70 m (Fig. 9). This may not only indicate the reliability in recording of the M/B boundary but it also suggests a similar

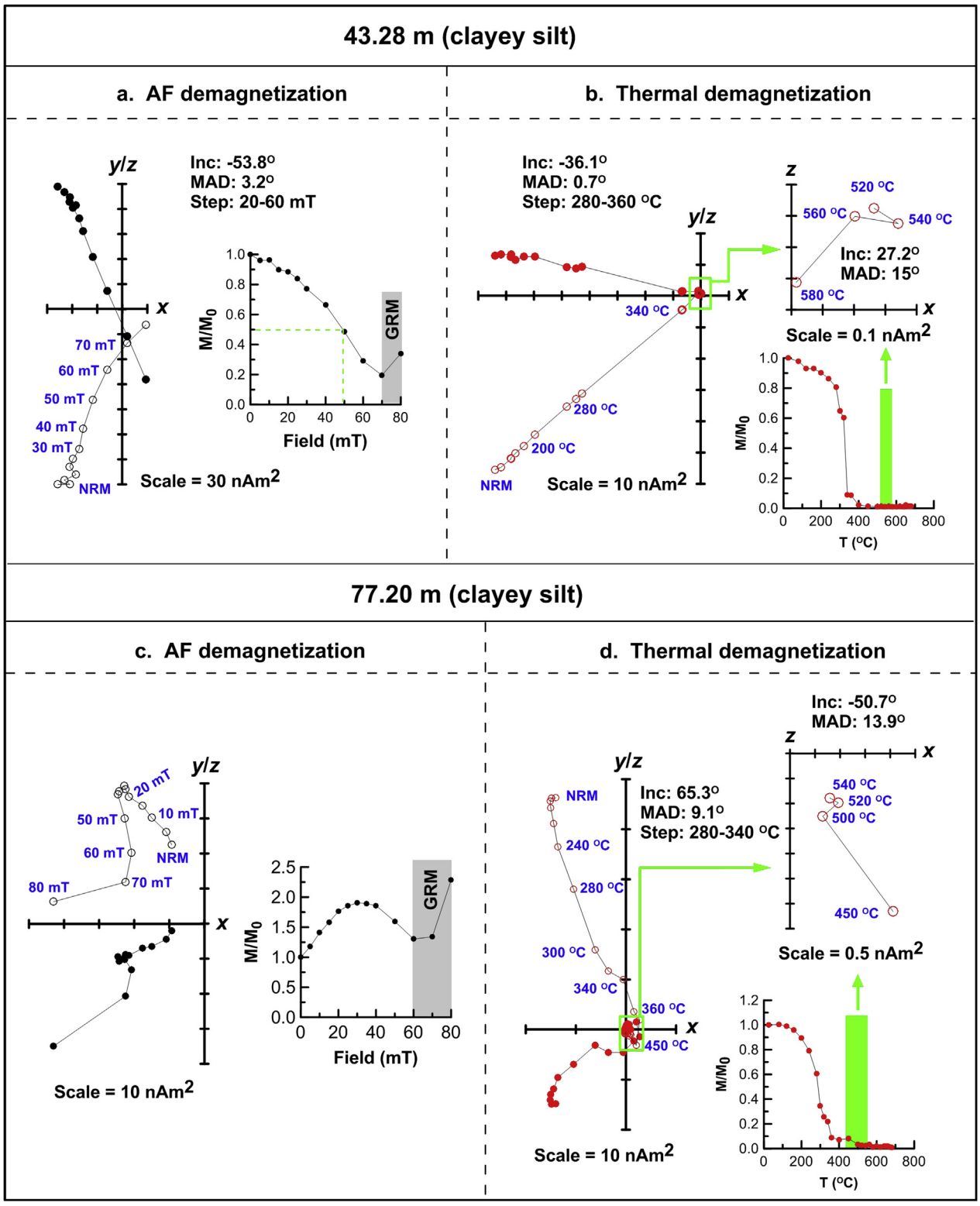

Fig. 6. Orthogonal vector plots and remanence decay curves for (a,c) stepwise AF and (b,d) thermal demagnetization data for representative greigite-bearing samples. The green dashed line in the remanence decay curve in (a) also denotes the median destructive field (MDF). Acquisition of a GRM is observed at high static AFs (grey bars in a, c), and high-temperature components due to magnetite often have contrasting polarities to those due to greigite (b,d). (For interpretation of the references to color in this figure caption, the reader is referred to the web version of this article.)

sedimentary history among the studied sites during this period. In addition, in view of the similar position and water depth of cores CSDP-1 and QC2 (Fig. 1b), correlation of the normal polarity magnetozone at around 112 m in core CSDP-1 (n2 in Fig. 7b) to the Jaramillo subchron further indicates that a much older basal age might also be present in core QC2 (Liu et al., 2014a).

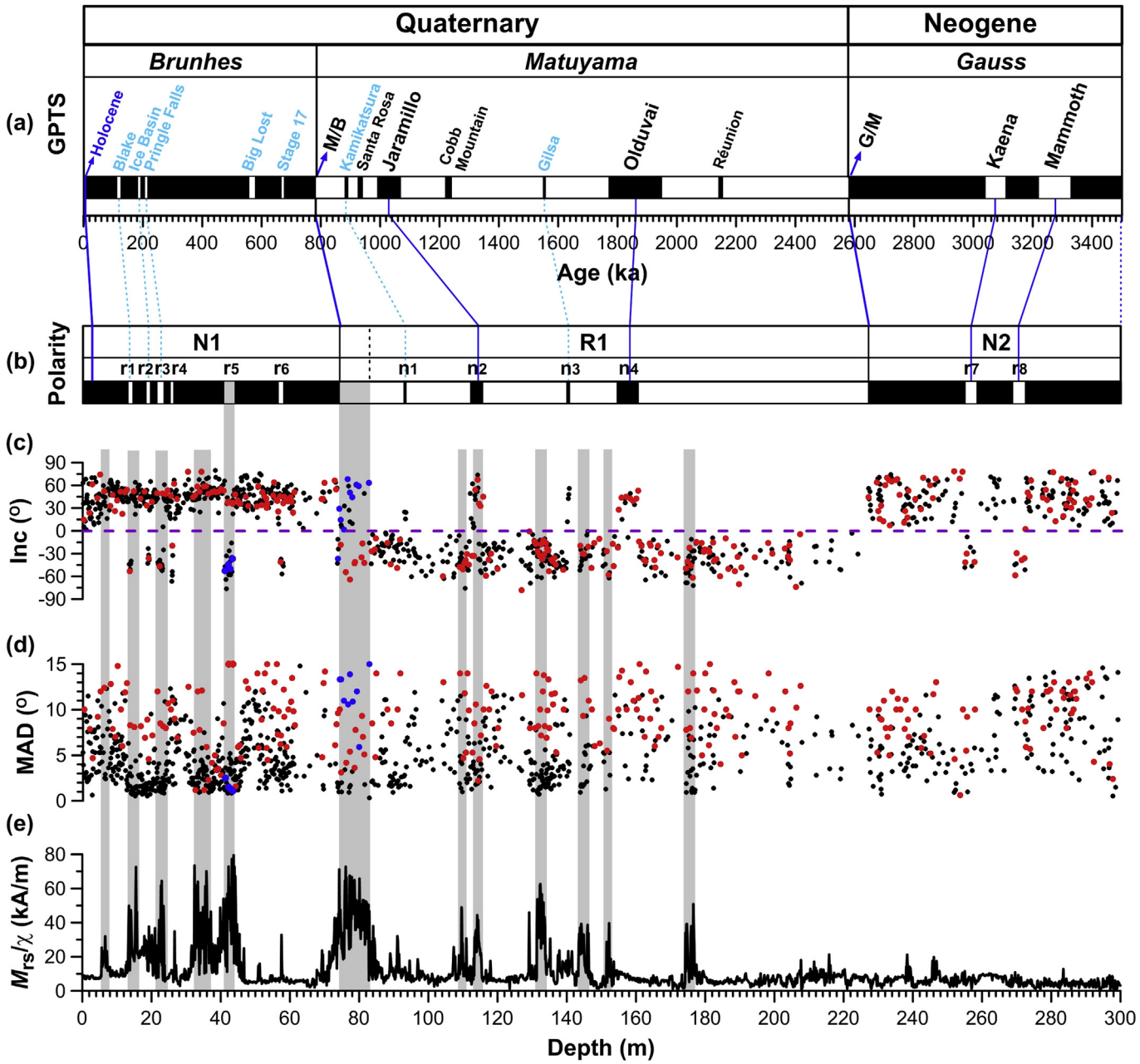

Fig. 7. Magnetostratigraphy of core CSDP-1. (a) Geomagnetic polarity time scale (GPTS) (Gradstein et al., 2012), the validated excursions marked with blue are from Laj and Channell (2007) and Roberts (2008), and reversals are marked with black. Variations of (b) polarity, (c–d) inclinations and maximum angle deviations (MAD), and (e) ratios of saturation remanence (M_{rs}) to magnetic susceptibility (χ: mass-specific) along the studied core. The black dots in (c) and (d) denote inclinations and MAD values calculated from AF demagnetization data, while red/blue dots denote thermal demagnetization data after/prior to 400 °C. The grey bars mark the greigite-bearing layers in the core, where high M_{rs}/χ values are taken to indicate SD-like properties due to greigite (Snowball, 1991; Roberts and Turner, 1993). (For interpretation of the references to color in this figure caption, the reader is referred to the web version of this article.)

With this new chronological framework for the core CSDP-1, the following issues can be clarified for the first time. First, the continental shelf of the East China Sea is the northernmost part of the Chinese continental shelf in which the base of the Quaternary has been recovered, and the bases of the Quaternary in the Yellow Sea and Bohai Sea have remained unknown for a long time (He, 2006). CSDP-1 is also the first core to recover the base of the Quaternary in the Yellow Sea, which will greatly promote studies of the evolution of the Yellow Sea on longer time scales.

The second issue concerns the occurrence time and extent of the first transgression of the Yellow Sea. According to geophysical data, the Fujian-Lingnan Uplift (FLU), which lies between the southeastern Korean Peninsula and the Yangtze Estuary (see the boundary dividing the SYS and East China Sea in Fig. 1b), has blocked the East China Sea from intruding into the Yellow Sea (Wageman et al., 1970). The FLU was reported to have subsided in the early Pleistocene, which allowed sea water ingression into the Yellow Sea, and several transgressions have subsequently occurred (Qin et al., 1989). Nevertheless, the details of these transgressions have not been well investigated due to the lack of chronological data (Qin et al., 1989).

Our study reveals that the upper 85-m of the studied core

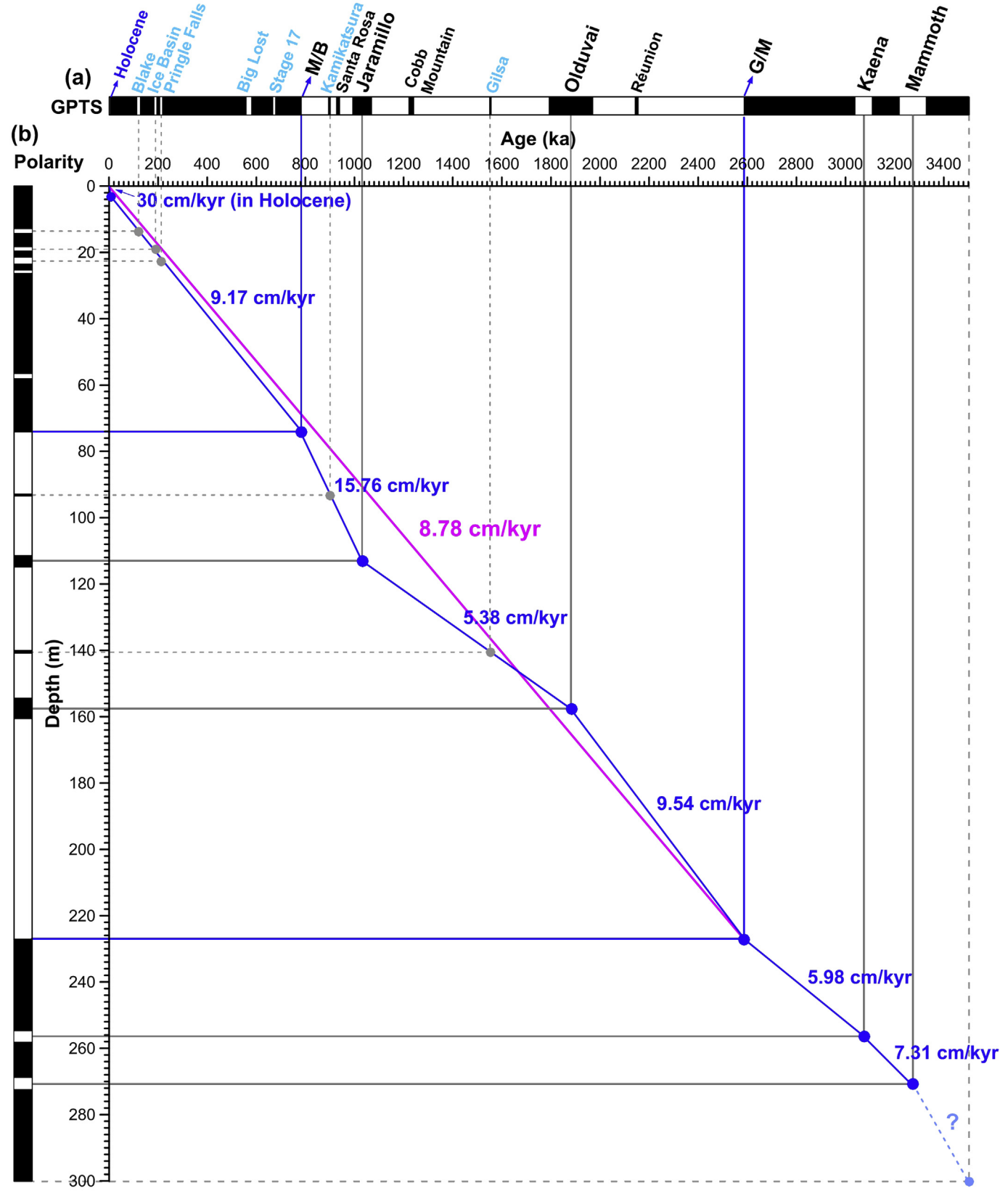

Fig. 8. Age-depth relationship for core CSDP-1, with (b) polarity correlating to the (a) GPTS (as shown in Fig. 7a). Only the age points of AMS ^{14}C dating and major polarity transitions and subchrons (blue dots) are used to calculate the sedimentation rates (in cm/kyr). (For interpretation of the references to color in this figure caption, the reader is referred to the web version of this article.)

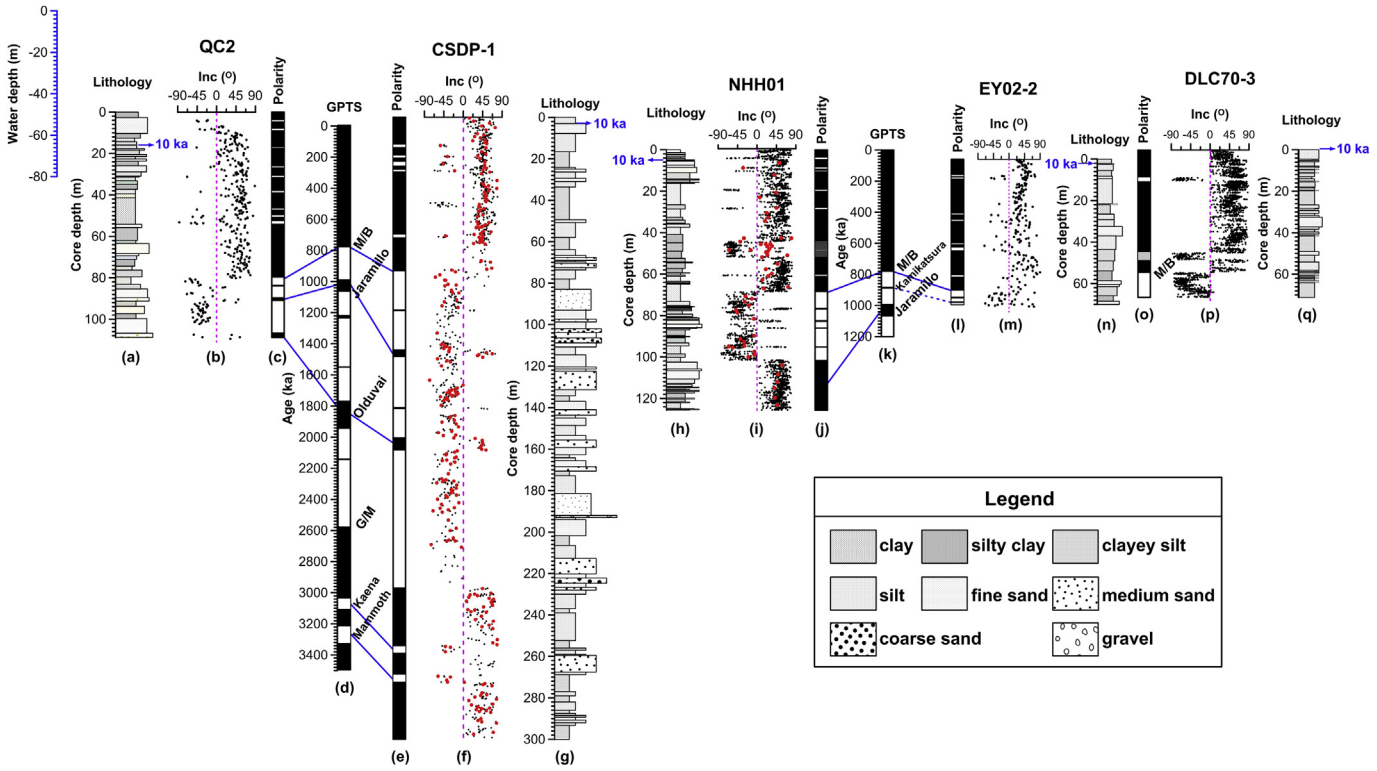

Fig. 9. Magnetostratigraphic frames including variations of (a, g, h, n, q) lithology, (b, f, i, m, p) inclinations, and (c, e, j, l, o) polarity along depths of existing long sediment cores from the SYS. The (d, k) GPTS is from Gradstein et al. (2012). Data for (a–c) core QC2 are from Zhou and Ge (1990), (l–n) EY02-2 from Ge et al. (2006), (h–j) NHH01 from Liu et al. (2014a), and (o–q) DLC70-3 from Mei et al. (2015). The ages "10 ka" marked with blue near the top of the cores were obtained via ^{14}C dating. The red dots in (f) and (i) denote inclinations calculated from thermal demagnetization data, and the black dots in (b, f, i, m, p) denote inclinations calculated from AF demagnetization data.

contains marine sediments. Three thin (less than 5 m) layers at depths of around 112 m, 135 m, and 145 m contain greigite, which were likely to have formed as a result of rapid sea-level change in the continental shelf sediments (e.g., Oda and Torii, 2004). Therefore, the occurrence age for the first marine deposit at depth of 145 m is ~1.7 Ma; two short-lived marine transgressions then occurred at ~1.44 Ma (135 m) and 1.03 Ma (112 m), respectively (Fig. 10c, d). These early transgressions of the Yellow Sea were characterized by short durations over small areas (Qin et al., 1989). Subsequently, seawater retreated until ~0.85 Ma. Then an extended marine transgression occurred again to create marine environments in the study area since ~0.7 Ma (Fig. 10c, d).

Studies of nearby core NHH01 (Fig. 1b) indicate that it records mostly marine environments since ~1.02 Ma (Fig. 10d, e) (Liu et al., 2014a), which along with core CSDP-1 indicate that the paleoshoreline probably lay between these two cores between ~1.02 Ma and ~0.85 Ma. The disparate thicknesses of the Jaramillo subchron in the two cores could be because core NHH01 was closer to the basin depocenter (Qin et al., 1989) for longer than core CSDP-1 during this period. In addition, several large amplitude sea-level regressions occurred in glacial periods such as during MIS 20, MIS 18, and MIS 10 (Fig. 10c–e), with seawater even retreating from the central SYS, which resulted in deposition of terrestrial sediments or erosion.

The third issue involves the effects of local tectonics on the depositional history of the SYS. Although climate has undoubtedly played an important role in evolution of the sedimentary environment of the Yellow Sea (Qin et al., 1989; He, 2006; Liu et al., 2010), it can not be the only driving factor in sedimentation. The lowest stand of sea-level is reported to be about −130 m in the Quaternary (Fig. 10c) (Miller et al., 2005; Rohling et al., 2009). If only climate is considered, sediments below depths of ~80 m in core CSDP-1 and ~60 m in core NHH01 should be marine deposits at least in interglacials since the first marine transgression into the SYS. This, however, is not the case (Fig. 10c, e). Therefore, the effects of local tectonic movements such as basement uplift or FLU after its first subsidence as Jin and Yu (1982) hypothesized, which warrant further investigation, should be given greater consideration in future. For the thicknesses of marine sediments documented in these cores to be present, the continental shelf must have undergone substantial subsidence coincident with sedimentation.

6. Conclusions

Systematic rock magnetic analyses on the longest sediment core (CSDP-1) yet recovered from the South Yellow Sea indicate that the magnetic minerals in the core consist of magnetite, greigite, and hematite, which occur either as the major magnetic carrier or they co-exist. The complexity of magnetic mineral assemblages in these continental shelf sediments, including remanences recorded by authigenic greigite, has a considerable influence on determination of a polarity stratigraphy, which is avoided by thermal demagnetization above 400 °C where no influence of greigite remains. The variable directions of these remanences further support the 'magnetic interaction-induced contradictory magnetization' mechanism. The M/B boundary is located at a depth of 73.68 m in the studied core, and the base of the Quaternary in the Yellow Sea has been recovered for the first time, which corresponds to a depth of 227.16 m in the studied core. The extrapolated basal age of the core is ~3.50 Ma. The first marine transgression into the Yellow Sea occurred no later than ~1.7 Ma, with other early transgressions characterized by short durations over small areas. Terrestrial

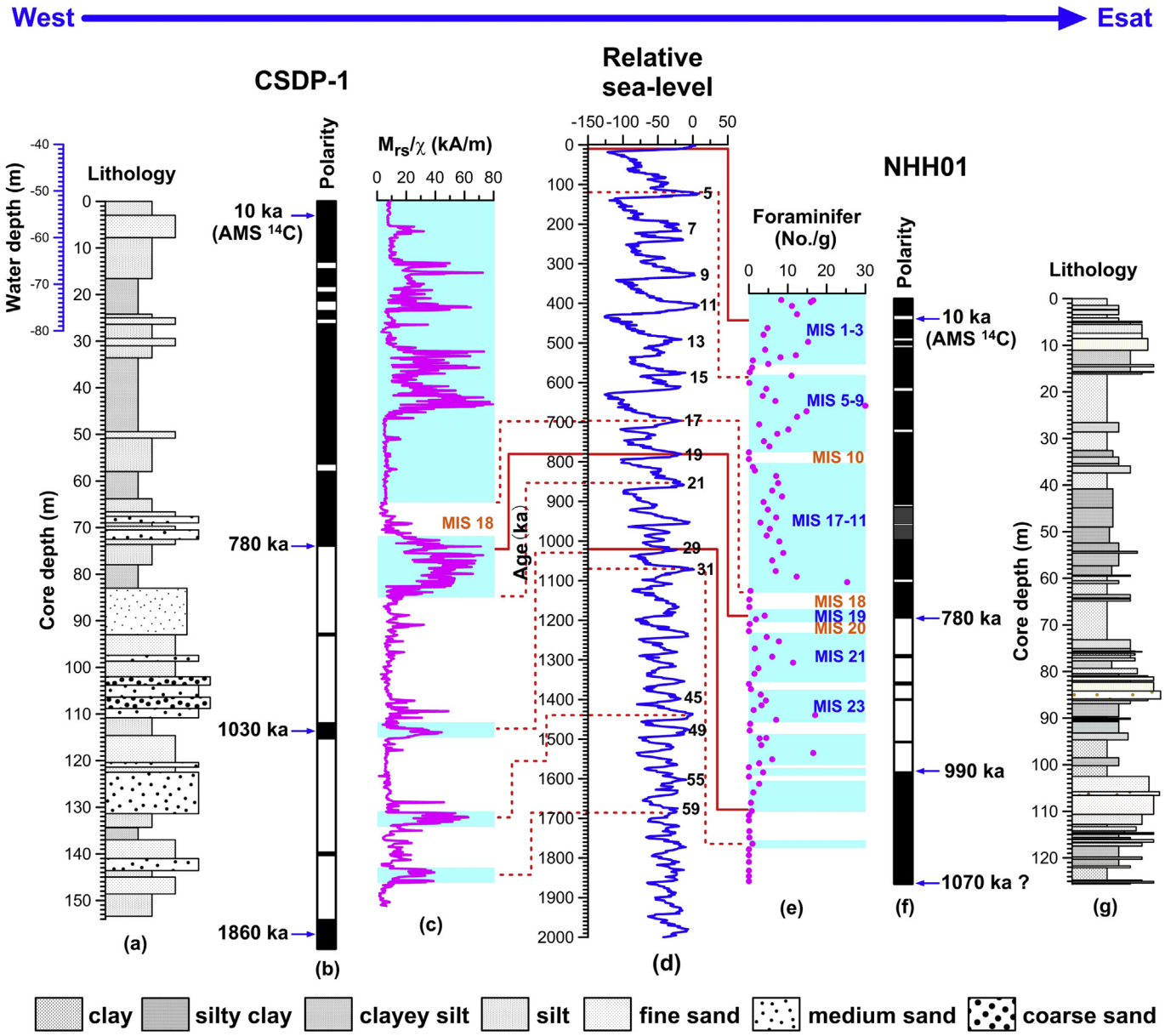

Fig. 10. Diagrammatic sketch for sedimentary evolution history of the Yellow Sea constructed from cores (a–c) CSDP-1 and (e–g) NHH01 (Liu et al., 2014a). Data for (d) relative sea-levels are from Miller et al. (2005). The blue bars in (c, e) denote marine deposits in the cores. Since marine deposits are only identified in the upper half of core CSDP-1, the lower section here is not displayed. (For interpretation of the references to color in this figure caption, the reader is referred to the web version of this article.)

deposition or erosion occurred in several glacial periods such as during MIS 20, MIS 18, and MIS 10 when seawater retreated from the central Yellow Sea. Both climate changes and local tectonics have controlled the evolution of sedimentation in the Yellow Sea throughout the Quaternary.

Acknowledgements

We are grateful to the reviewers and the Editor for their thoughtful and constructive comments and suggestions that greatly improved the manuscript. We thank the crew of the R/V *Kan407* for their assistance with core drilling. Sincere appreciation is expressed to Qiongyi Luo, Jie Li, Debo Zhao, Jin Zhang, and Zhongya Chen for their help with sampling. This work was jointly supported by the China Geological Survey (No. GZH201100202), the National Natural Science Foundation of China (No. 41430962), the Project of Taishan Scholar (No. 41330964), and Project of State Oceanic Administration, China (No. 908-01-BC15).

Appendix A. Supplementary data

Supplementary data related to this article can be found at http://dx.doi.org/10.1016/j.quascirev.2016.05.025.

References

Benning, L.G., Wilkin, R.T., Barnes, H.L., 2000. Reaction pathways in the Fe-S system below 100 °C. Chem. Geol. 167, 25–51.
Berner, R.A., 1984. Sedimentary pyrite formation: an update. Geochim. Cosmochim. Acta 48, 605–615.
Canfield, D.E., Berner, R.A., 1987. Dissolution and pyritization of magnetite in anoxic marine sediments. Geochim. Cosmochim. Acta 51, 645–659.
Chang, L., Roberts, A.P., Tang, Y., Rainford, B.D., Muxworthy, A.R., Chen, Q., 2008. Fundamental magnetic parameters from pure synthetic greigite (Fe_3S_4).

J. Geophys. Res. 113, B06104. http://dx.doi.org/10.1029/2007JB005502.
Dunlop, D.J., Özdemir, Ö., 1997. Rock Magnetism: Fundamentals and Frontiers. Cambridge University Press, New York, p. 573.
Eckert, R.D., 1979. The Enclosure of Ocean Resources: Economics and the Law of the Sea. Hoover Institution Press, Stanford, Calif.
Florindo, F., Sagnotti, L., 1995. Palaeomagnetism and rock magnetism in the upper Pliocene Valle Ricca (Rome, Italy) section. Geophys. J. Int. 123, 340–354.
Fu, Y.Z., von Dobeneck, T., Franke, C., Heslop, D., Kasten, S., 2008. Rock magnetic identification and geochemical process models of greigite formation in Quaternary marine sediments from the Gulf of Mexico (IODP Hole U1319A). Earth Planet. Sci. Lett. 275, 233–245.
Ge, S.L., Shi, X.F., Zhu, R.X., Liu, Y.G., Yin, P., Liu, L.J., 2006. Magnetostratigraphy of borehole EY02-2 in the southern Yellow Sea and its paleoenvironmental significance. Chin. Sci. Bull. 51, 855–865.
Gerber, T.P., Pratson, L.F., Kuehl, S., Walsh, J.P., Alexander, C., Palmer, A., 2010. The influence of sea level and tectonics on Late Pleistocene through Holocene sediment storage along the high-sediment supply Waipaoa continental shelf. Mar. Geol. 270, 139–159.
Gradstein, F.M., Ogg, J.G., Schmitz, M.D., Ogg, G.M., 2012. The Geologic Time Scale. Elsevier, U.K., p. 1144
Harrison, R.J., Feinberg, J.M., 2008. FORCinel: an improved algorithm for calculating first-order reversal curve distributions using locally weighted regression smoothing. Geochem. Geophys. Geosyst. 9, Q05016. http://dx.doi.org/10.1029/2008GC001987.
He, Q.X., 2006. Marine Sedimentary Geology of China. China Ocean Press, Beijing, pp. 171–175 (in Chinese).
Hirt, A.M., Gehring, A.U., 1991. Thermal alteration of the magnetic mineralogy in ferruginous rocks. J. Geophys. Res. 96, 9947–9953.
Hirt, A.M., Banin, A., Gehring, A.U., 1993. Thermal generation of ferromagnetic minerals from iron-enriched smectites. Geophys. J. Int. 115, 1161–1168.
Horng, C.-S., Torii, M., Shea, K.-S., Lee, T.Q., 1998. Inconsistent magnetic polarities between greigite- and pyrrhotite/magnetite-bearing marine sediments from the Tsailiao-chi section, southwest Taiwan. Earth Planet. Sci. Lett. 164, 467–481.
Hrouda, F., 1982. Magnetic anisotropy of rocks and its application in geology and geophysics. Surv. Geophys. 5, 37–82.
Hrouda, F., 1994. A technique for the measurement of thermal changes of magnetic susceptibility of weakly magnetic rocks by the CS-2 apparatus and KLY-2 Kappabridge. Geophys. J. Int. 118, 604–612.
Jiang, W.T., Horng, C.-S., Roberts, A.P., Peacor, D.R., 2001. Contradictory magnetic polarities in sediments and variable timing of neoformation of authigenic greigite. Earth Planet. Sci. Lett. 193, 1–12.
Jin, X.L., Yu, P.Z., 1982. Tectonics of the Yellow Sea and the East China Sea. In: The Geology of the Yellow Sea and the East China Sea. China Ocean Press, Beijing, pp. 1–22 (in Chinese).
Kim, D., Park, B.K., Shin, I.C., 1999. Paleoenvironmental changes of the Yellow Sea during the late Quaternary. Geo Mar. Lett. 18, 189–194.
Kirschvink, J.L., 1980. The least-square line and plane and the analysis of palaeomagnetic data. Geophys. J. R. Astron. Soc. 62, 699–718.
Laj, C., Channell, J.E.T., 2007. Geomagnetic excursions. In: Kono, M. (Ed.), Geomagnetism Treatise on Geophysics, vol. 5, pp. 373–416.
Lan, X.H., Zhang, X.H., Zhang, Z.X., 2005. Material sources and transportation of sediments in the southern Yellow Sea. Trans Oceanol. Limnol. 4, 53–60 (in Chinese with English abstract).
Lanci, L., Pares, J.M., Channell, J.E.T., Kent, D.V., 2004. Miocene magnetostratigraphy from equatorial Pacific sediments (ODP Site 1218, Leg 199). Earth Planet. Sci. Lett. 226, 207–224.
Larrasoaña, J.C., Roberts, A.P., Musgrave, R.J., Gràcia, E., Piñero, E., Vega, M., Martínez-Ruiz, F., 2007. Diagenetic formation of greigite and pyrrhotite in gas hydrate marine sedimentary systems. Earth Planet. Sci. Lett. 261, 350–366.
Liu, J., Zhu, R.X., Roberts, A.P., Li, S.Q., Chang, J.-H., 2004. High-resolution analysis of early diagenetic effects on magnetic minerals in post-middle-Holocene continental shelf sediments from the Korea Strait. J. Geophys. Res. 109, B03103. http://dx.doi.org/10.1029/2003JB002813.
Liu, J., Satio, Y., Kong, X.H., Wang, H., Wen, Z., Yang, Z.G., Nakashima, R., 2010. Delta development and channel incision during marine isotope stages 3 and 2 in the western South Yellow Sea. Mar. Geol. 278, 54–76.
Liu, J.X., Shi, X.F., Liu, Q.S., Ge, S.L., Liu, Y.G., Yao, Z.Q., Zhao, Q.H., Jin, C.S., Jiang, Z.X., Liu, S.F., Qiao, S.Q., Li, X.Y., Li, C.S., Wang, C.J., 2014a. Magnetostratigraphy of a greigite-bearing core from the South Yellow Sea: implications for remagnetization and sedimentation. J. Geophys. Res. 119, 7425–7441.
Liu, J.X., Shi, X.F., Ge, S.L., Liu, Q.S., Yao, Z.Q., Yang, G., 2014b. Identification of the thick-layer greigite in sediments of the South Yellow Sea and its geological significances. Chin. Sci. Bull. 59, 2764–2775.
Lowrie, W., 1990. Identification of ferromagnetic minerals in a rock by coercivity and unblocking temperature properties. Geophys. Res. Lett. 17, 159–162.
McMillan, A.A., 2002. Onshore Quaternary geological surveys in the 21st century-a perspective from the British Geological Survey. Quat. Sci. Rev. 21, 889–899.
Mei, X., Li, R.H., Zhang, X.H., Liu, Q.S., Liu, J.X., Wang, Z.B., Lan, X.H., Liu, J., Sun, R.T., 2016. Evolution of the Yellow Sea warm current and the Yellow Sea cold water mass since the Middle Pleistocene. Palaeogeogr. Palaeoclimatol. Palaeocol. 442, 48–60.
Miller, K.G., Kominz, M.A., Browning, J.V., Wright, J.D., Mountain, G.S., Katz, M.E., Sugarman, P.J., Gramer, B.S., Christie-Blick, N., Pekar, S.F., 2005. The Phanerozoic record of global sea-level change. Science 310, 1293–1298.
Muxworthy, A.R., Dunlop, D.J., 2002. First-order reversal curve (FORC) diagrams for pseudo-single-domain magnetites at high temperature. Earth Planet. Sci. Lett. 203, 369–382.
Nilsson, A., Lee, Y.S., Snowball, I., Hill, M., 2013. Magnetostratigraphic importance of secondary chemical remanent magnetizations carried by greigite (Fe_3S_4) in Miocene sediments, New Jersey shelf (IODP Expedition 313). Geosphere 9, 510–520.
Oda, H., Torii, M., 2004. Sea-level change and remagnetization of continental shelf sediments off New Jersey (ODP Leg 174A): magnetite and greigite diagenesis. Geophys. J. Int. 156, 443–458.
O'Reilly, W., Banerjee, S.K., 1966. Oxidation of titanomagnetites and self-reversal. Nature 211, 26–28.
Passier, H.F., de Lange, G.J., Dekkers, M.J., 2001. Magnetic properties and geochemistry of the active oxidation front and the youngest sapropel in the eastern Mediterranean Sea. Geophys. J. Int. 145, 604–614.
Pike, C.R., Roberts, A.P., Verosub, K.L., 1999. Characterizing interactions in fine magnetic particle systems using first order reversal curves. J. Appl. Phys. 85, 6660–6667.
Qin, H.F., Liu, Q.S., Pan, Y.X., 2008. The first-order reversal curve (FORC) diagram: theory and case study. Chin. J. Geophys. 51, 743–751 (in Chinese).
Qin, Y.S., Zhao, Y.Y., Chen, L.R., Zhao, S.L., 1989. Geology of the Yellow Sea. China Ocean Press, Beijing, 1–289 (in Chinese).
Reynolds, R.L., Rosenbaum, J.G., van Metre, P., Tuttle, M., Callender, E., Goldin, A., 1999. Greigite as an indicator of drought –the 1912-1994 sediment magnetic record from White Rock Lake, Dallas, Texas, USA. J. Paleolimnol. 21, 193–206.
Roberts, A.P., Turner, G.M., 1993. Diagenetic formation of ferrimagnetic iron sulphide minerals in rapidly deposited marine sediments, South Island, New Zealand. Earth Planet. Sci. Lett. 115, 257–273.
Roberts, A.P., 1995. Magnetic properties of sedimentary greigite (Fe_3S_4). Earth Planet. Sci. Lett. 134, 227–236.
Roberts, A.P., Cui, Y., Verosub, K.L., 1995. Wasp-waisted hysteresis loops: mineral magnetic characteristics and discrimination of components in mixed magnetic systems. J. Geophys. Res. 100, 17909–17924.
Roberts, A.P., Pike, C.R., Verosub, K.L., 2000. FORC diagrams: a new tool for characterizing the magnetic properties of natural samples. J. Geophys. Res. 105, 28461–28475.
Roberts, A.P., Jiang, W.-T., Florindo, F., Horng, C.-S., Laj, C., 2005. Assessing the timing of greigite formation and the reliability of the Upper Olduvai polarity transition record from the Crostolo River, Italy. Geophys. Res. Lett. 32, L05307. http://dx.doi.org/10.1029/2004GL022137.
Roberts, A.P., Weaver, R., 2005. Multiple mechanisms of remagnetization involving sedimentary greigite (Fe_3S_4). Earth Planet. Sci. Lett. 231, 263–277.
Roberts, A.P., Liu, Q.S., Rowan, C.J., Chang, L., Carvallo, C., Torrent, J., Horng, C.-S., 2006. Characterization of hematite (α-Fe_2O_3), geothite (α-FeOOH), greigite (Fe_3S_4), and pyrrhotite (Fe_7S_8) using first-order reversal curve diagrams. J. Geophys. Res. 111, B12S35. http://dx.doi.org/10.1029/2006/JB004715.
Roberts, A.P., 2008. Geomagnetic excursions: knowns and unknowns. Geophys. Res. Lett. 35, L17307. http://dx.doi.org/10.1029/2008GL034719.
Roberts, A.P., Chang, L., Rowan, C.J., Horng, C.-S., Florindo, F., 2011. Magnetic properties of sedimentary greigite (Fe_3S_4): an update. Rev. Geophys. 49, RG1002. http://dx.doi.org/10.1029/2010RG000336.
Roberts, A.P., Heslop, D., Zhao, X., Pike, C.R., 2014. Understanding fine magnetic particle systems through use of first-order reversal curve diagrams. Rev. Geophys. 52 http://dx.doi.org/10.1002/2014RG000462.
Roberts, A.P., 2015. Magnetic mineral diagenesis. Earth Sci. Rev. 151, 1–47.
Rohling, E.J., Grant, K., Bolshaw, M., Roberts, A.P., Siddall, M., Hemleben, Ch, Kucera, M., 2009. Antarctic temperature and global sea level closely coupled over the past five glacial cycles. Nat. Geosci. 2, 500–504.
Sagnotti, L., Roberts, A.P., Weaver, R., Verosub, K.L., Florindo, F., Pike, C.R., Clayton, T., Wilson, G.S., 2005. Apparent magnetic polarity reversals due to remagnetization resulting from late diagenetic growth of greigite from siderite. Geophys. J. Int. 160, 89–100.
Sagnotti, L., Cascella, A., Ciaranfi, N., Macrì, P., Maiorano, P., Marino, M., Taddeucci, J., 2010. Rock magnetism and palaeomagnetism of the Montalbano Jonico section (Italy): evidence for late diagenetic growth of greigite and implications for magnetostratigraphy. Geophys. J. Int. 180, 1049–1066.
Schult, A., 1968. Self-reversal of magnetization and chemical composition of titanimagnetites in basalts. Earth Planet. Sci. Lett. 4, 57–63.
Snowball, I.F., 1991. Magnetic hysteresis properties of greigite (Fe_3S_4) and a new occurrence in Holocene sediments from Swedish Lappland. Phys. Earth Planet. Inter. 68, 32–40.
Snowball, I.F., 1997. Gyroremanent magnetization and the magnetic properties of greigite-bearing clays in southern Sweden. Geophys. J. Int. 129, 624–636.
Tauxe, L., Stickley, C.E., Sugisaki, S., et al., 2012. Chronostratigraphic framework for the IODP expedition 318 cores from the Wilkes land margin: constraints for paleoceanographic reconstruction. Paleoceanography 27, PA2214. http://dx.doi.org/10.1029/2012PA002308.
Troiani, B.T., Simms, A.R., Dellapenna, T., Piper, E., Yokoyama, Y., 2011. The importance of sea-level and climate change, including changing wind energy, on the evolution of a coastal estuary: Copano Bay, Texas. Mar. Geol. 280, 1–19.
Verwey, E.J.W., 1939. Electronic conduction of magnetite (Fe_3O_4) and its transition point at low-temperature. Nature 144, 327–328.
Wageman, J.M., Hilde, T.W.C., Emery, K.O., 1970. Structural framework of the East China Sea and Yellow Sea. AAPG Bull. 54, 1611–1643.
Xiang, R., Yang, Z.S., Satio, Y., Fan, D.J., Chen, M.H., Guo, Z.G., Chen, Z., 2008. Paleoenvironmental changes during the last 8400 years in the southern Yellow Sea:

benthic foraminifera and stable isotopic evidence. Mar. Micropaleontol. 67, 104–119.
Yang, S.Y., Jung, H.S., Lim, D.I., Li, C.X., 2003. A review on the provenance discrimination of sediments in the Yellow Sea. Earth Sci. Rev. 63, 93–120.
Yang, Z.G., 1993. The sedimentary sequence and palaeogeographic changes of the South Yellow Sea since the Olduvai subchron. Acta Geol. Sin. 67, 357–366 (in Chinese with English abstract).
Yang, Z.G., Lin, H.M., Zhang, G.W., 1996. In: Yang, Z.G., Lin, H.M. (Eds.), The Quaternary Sequences in the Continental Shelf of the Yellow Sea, the Quaternary Sequences and International Correlation. China Geology Press, Beijing, pp. 31–55 (in Chinese).
Yang, Z.S., Liu, J.P., 2007. A unique Yellow River-derived subaqueous delta in the Yellow Sea. Mar. Geol. 240, 169–176.
Yao, Z.Q., Shi, X.F., Liu, Q.S., Liu, Y.G., Larrasoaña, J.C., Liu, J.X., Ge, S.L., Wang, K.S., Qiao, S.Q., Li, X.Y., Shi, F.D., Fang, X.S., Yu, Y.G., Yang, G., Duan, Z.Q., 2014. Paleomagnetic and astronomical dating of sediment core BH08 from the Bohai Sea, China: implications for glacial-interglacial sedimentation. Palaeogeogr. Palaeoclimatol. Palaeocol. 393, 90–101.
Zheng, Z., Zhao, X.X., Horng, C.-S., 2010. A new high-precision furnace for paleomagnetic and paleointensity studies: minimizing magnetic noise generated by heater currents inside traditional thermal demagnetizers. Geochem. Geophys. Geosyst. 11, Q04Y08. http://dx.doi.org/10.1029/2010GC003100.
Zhou, M.Q., Ge, Z.S., 1990. The magnetostratigraphy of unconsolidated sediments in the southern Yellow Sea and adjacent areas. Mar. Geol. Quat. Geol. 10, 21–33 (in Chinese with English abstract).
Zijderveld, J.D.A., 1967. A.C. demagnetization of rocks: analysis of results. In: Collinson, D.W., Creer, K.M., Runcorn, S.K. (Eds.), Methods in Paleomagnetism. Elsevier, New York, pp. 254–286.